Weierstraß-Institut

für Angewandte Analysis und Stochastik

Leibniz-Institut im Forschungsverbund Berlin e. V.

Preprint ISSN 2198 – 5855

Numerical simulations and measurements of a droplet size distribution in a turbulent vortex street

Ellen Schmeyer[1], Róbert Bordás[2], Dominique Thévenin[2] , Volker John[3]

submitted: January 8, 2014

[1] Weierstrass Institute
Mohrenstr. 39
10117 Berlin
Germany
email: ellen.schmeyer@wias-berlin.de

[2] University of Magdeburg “Otto von Guericke”
Universitätsplatz 2
39106 Magdeburg, Germany
email: bordas@ovgu.de
email: thevenin@ovgu.de

[3] Weierstrass Institute
Mohrenstr. 39, 10117 Berlin, Germany
and Free University of Berlin
Dep. of Mathematics and Computer Science
Arnimallee 6, 14195 Berlin, Germany
email: volker.john@wias-berlin.de

No. 1917

Berlin 2014

2010 *Mathematics Subject Classification.* 76F65, 76T10.

Key words and phrases. two-phase turbulent vortex street, disperse droplet population, non-intrusive measurements, population balance systmes, direct discretizations.

Edited by
Weierstraß-Institut für Angewandte Analysis und Stochastik (WIAS)
Leibniz-Institut im Forschungsverbund Berlin e. V.
Mohrenstraße 39
10117 Berlin
Germany

Fax: +49 30 20372-303
E-Mail: preprint@wias-berlin.de
World Wide Web: http://www.wias-berlin.de/

Abstract

A turbulent vortex street in an air flow interacting with a disperse droplet population is investigated in a wind tunnel. Non-intrusive measurement techniques are used to obtain data for the air velocity and the droplet velocity. The process is modeled with a population balance system consisting of the incompressible Navier–Stokes equations and a population balance equation for the droplet size distribution. Numerical simulations are performed that rely on a variational multiscale method for turbulent flows, a direct discretization of the differential operator of the population balance equation, and a modern technique for the evaluation of the coalescence integrals. After having calibrated two unknown model parameters, a very good agreement of the experimental and numerical results can be observed.

Eine turbulente Wirbelstraße in einer Luftströmung mit einer dispergierten Tröpfchenpopulation wird in einem Windkanal untersucht. Nichtintrusive Messtechniken werden verwendet, um Daten bezüglich der Luft– und Tröpfchengeschwindigkeiten zu gewinnen. Der zu Grunde liegende Prozess wird mit einem Populationsbilanzsystem modelliert, welches aus den inkompressiblen Navier–Stokes–Gleichungen und einer Populationsbilanzgleichung für die Tröpfchenverteilungsdichte besteht. Numerische Simulationen werden durchgeführt, welche ein variationelle Mehrskalenmethode für turbulente Strömungen, eine direkte Diskretisierung des Differentialoperators der Populationsbilanzgleichung und ein modernes Verfahren zur Berechnung der Koaleszensintegrale verwenden. Nachdem zwei unbekannte Modellparameter kalibriert worden sind, kann eine sehr gute Übereinstimmung der experimentellen und numerischen Ergebnisse beobachtet werden.

1 Introduction

An active field of research in meteorology is the evolution of clouds. Since an enormous difficulty consists in obtaining reliable data from nature, a straightforward approach consists in performing wind tunnel experiments that represent some important properties of clouds. Based on available experimental data, models and numerical methods can be studied for their ability to reproduce these data and therefore to be potential candidates for the modeling and simulation of clouds. This paper presents a study that includes experiments, modeling, and numerical simulations.

Clouds can be thought of as consisting of small water droplets moving in air. The motion of the air is often turbulent and it causes frequent droplet-droplet interactions. The performed wind tunnel experiments focused exactly on this feature. In first experiments, described in detail in Bordás et al. (2011, 2012, 2013b), a turbulent channel flow was considered. This type of flow is one of the simplest turbulent flows and it is characterized by the absence of large coherent eddies. In Bordás et al. (2012, 2013a), a research program containing experiments, modeling, and numerical simulations was performed for this type of flow. In particular, a number of numerical methods were identified such that a good agreement of experimental and numerical results could be obtained. However, large coherent eddies might be present in turbulent flows in clouds. For this reason, a second experiment was designed, which led to the formation of large coherent eddies (large with respect to the diameter of the droplets). To this end, a cylinder was inserted into the wind tunnel such that the formation of a turbulent Kármán vortex street was caused. The current paper considers this configuration.

Water droplets were injected into a Göttingen-type wind tunnel with a closed test section. In between the injection point and the test section, the cylinder was inserted. Experimental data of both phases, e.g., velocities of air and droplets, were determined with non-intrusive measurement techniques. These time-averaged data were used as boundary conditions for the model and for comparison with the results from the numerical simulations. All measurement data are collected in an online database accessible at http://www.ovgu.de/isut/lss/metstroem. The considered process can be found as M3 in this database. The raw measurement results were further post-processed, so that all required data are in a suitable form for comparisons and validation.

The behavior of the air-droplet flow was modeled by means of a population balance system. The incompressible Navier–Stokes equations describe the motion of the turbulent flow field. They are coupled with a population balance equation for the droplet size distribution (DSD). Whereas the velocity and the pressure of the flow field depend on time and space, the DSD depends in addition on an internal coordinate, which is here the diameter of the droplets. In the used model, the transport of the droplets with the flow field, the growth of the droplets in supersaturated air, and the coalescence of droplets were considered. The chosen collision kernel has two unknown parameters.

There are several, principally different, approaches for the numerical simulation of population balance systems. Applying some time-stepping scheme, one has to solve in each discrete time a population balance equation that is defined in a 4D domain, spanned by the spatial coordinates and the internal coordinate. Popular approaches for dealing with this difficulty are momentum-based meth-

ods, in particular the direct quadrature method of moments (DQMOM) from Marchisio and Fox (2005). Also operator-splitting schemes have been proposed in Ganesan and Tobiska (2012). These two approaches reduce the complexity of the numerical solution of the 4D equation by solving problems in lower-dimensional domains instead. However, this reduction of complexity introduces some (unknown) error. With the rise of computer power in the last decade, also direct discretizations of the 4D equation became possible. Errors committed from complexity reduction are avoided in this approach. Direct discretizations of the equation for the DSD will be studied in the numerical simulations presented in this paper.

In recent years, we gained some experience with the approach of using direct discretizations, based on finite difference and finite element methods, see Bordás et al. (2012, 2013a); Hackbusch et al. (2012). In the numerical simulations presented in this paper, the best methods from these studies were applied. A main goal of the numerical simulations was the identification of the unknown model parameters from the collision kernel. This goal was achieved by calibrating experimental and numerical data. The basis of this calibration was a space-time averaged DSD at the outlet of the test section. In addition, the impact of different kinds of flows on the same DSD will be investigated numerically.

The paper is organized as follows. Section 2 describes the setup and the procedure for the measurements. The model of the process is introduced and discussed in Section 3. A short description of the numerical methods is provided in Section 4. The experimental and numerical results are presented in Section 5. The paper concludes with a summary and outlook in Section 6.

2 Measurement setup

A wind tunnel capable of generating a disperse two-phase flow, available at the University of Magdeburg "Otto von Guericke", has been used for the present measurements, roughly corresponding to conditions found in cumulus clouds as discussed in Bordás et al. (2011, 2013b). This wind tunnel is a fully computer-controlled, so-called Prandtl or Göttingen-type wind tunnel, shown in Fig. 1. The test section itself is of size height $\times$ width $\times$ length $= 0.5 \times 0.6 \times 1.5$ m. It includes transparent windows of size 0.45×0.5 m. In this manner, non-intrusive optical measurements are possible, which is essential for high-quality experimental investigations of such flows.

The present paper considers a configuration with a bluff body. It is a cylinder with a diameter of $D = 0.02$ m, fixed at the height of $z = +0.09$ m perpendicular to the main flow, right before the measurement section as shown in Fig. 1, right. For the reasons described in Bordás et al. (2012), the measurement area is finally restricted to the lower half of the cross-section in the wind tunnel. The longitudinal coordinate of the beginning of the measurement section was set to be $x = 0$ m. Different measurement planes perpendicular to the main flow direction were investigated, at $x = 0$ m, $x = 0.2$ m, and $x = 0.4$ m. The first plane at $x = 0$ m was measured particularly thoroughly, since it provided the information needed for the boundary condition of the numerical simulations.

The disperse phase was generated with the help of a spray system, actuated by means of eccentric screw pumps. The number of revolutions per minute of the pumps (rpm), needed to inject the required water volume flow rate, was

adjusted by a frequency regulator including a Proportional Integral Derivative (PID) regulation coded in LabView. In order to generate a typical cumulus cloud droplet spectrum, a full cone air-assisted atomizing nozzle was used (type 166.208.16.12, co. Lechler). The applied air gauge pressure was 1.2 bar.

Experimental measurements were systematically carried out by means of non-intrusive measurement techniques. Therefore, a small quantity of suitable tracer particles had to be added to the flow. Such particles follow the structures of the continuous phase much better than the considered droplets, allowing an indirect measure of the gas flow properties. For this reason, the velocities of both phases were measured in two separate steps.

3 The Model of the Process

The process was modeled via a population balance system consisting of the incompressible Navier–Stokes equations to describe the flow field and a population balance equation which describes the behavior of the droplet size distribution.

Considering first the flow field, the incompressible Navier–Stokes equations are given by

$$\begin{aligned} \partial_t \mathbf{u} - \nabla \cdot 2\nu\mathbb{D}(\mathbf{u}) + (\nabla \cdot \mathbf{u})\mathbf{u} + \frac{1}{\rho}\nabla p &= \mathbf{0} \quad \text{in } (0, t_e) \times \Omega_{\text{NSE}}, \\ \nabla \cdot \mathbf{u} &= 0 \quad \text{in } (0, t_e) \times \Omega_{\text{NSE}}, \end{aligned} \tag{1}$$

where $\mathbf{u}$ ($^{\text{m}}/_{\text{s}}$) is the velocity field, p (Pa) the pressure, $\rho = 1.2041$ $^{\text{kg}}/_{\text{m}^3}$ the density of dry air at 293.15 K, $\nu = 15.031 \cdot 10^{-6}$ $^{\text{m}^2}/_{\text{s}}$ the kinematic viscosity, Ω_{NSE} the flow domain, and t_e (s) denotes the final time. The velocity deformation tensor, which is the symmetric part of the velocity gradient, is denoted by $\mathbb{D}(\mathbf{u})$. Because of the low Mach number in the experiments, the density can be assumed to be constant. The term describing the gravitational acceleration was absorbed into the pressure.

The computational domain has to contain the cylinder and the measurement section. Measurements were performed only in the lower half of the wind tunnel such that the consideration of this half is sufficient. The inlet has to be chosen sufficiently away from the cylinder. In addition, a boundary condition for the air velocity at the last measurement plane was not known. In the numerical simulations, a standard outflow condition was applied. In order that this condition does not distort the computational results at this plane, the outlet of the computational domain was chosen to be somewhat behind this plane. Setting the origin of the coordinate system in the center of the wind tunnel at the location of the first measurement plane, the domain for the flow simulation was chosen to be

$$\Omega_{\text{NSE}} = (-0.3, 0.5) \times (-0.225, 0.225) \times (-0.18, 0) \text{ m}^3.$$

Appropriate boundary conditions and an initial condition are necessary to close the Navier–Stokes equations (1). As initial condition, a fully developed flow field, which was computed in a preprocessing step, was used. The boundary condition at the inflow boundary $\Gamma_{\text{in}} = \{-0.3\} \times (-0.225, 0.225) \times (-0.18, 0)$ was based on experimental data. Before reaching the cylinder, the flow is a channel flow as it was considered in Bordás et al. (2012, 2013a). Therefore, the

experimental inlet data for the flow from Bordás et al. (2012, 2013a) were used also in the simulations presented here. For this purpose, a time-averaged experimental velocity $\mathbf{u}_{\text{exp}}(-0.3, y, z)$ and the corresponding time-averaged standard deviation $\boldsymbol{\sigma}_{\text{exp}}(-0.3, y, z)$ were available. In the simulations, these data were disturbed with noise calculated with the method proposed in Klein et al. (2003). This method enables the calculation of a spatially and temporally correlated random variable, where the fluctuations of a point correlate with those of the same vortex. The integral length scales serve as measures for the vortex lengths. For the considered example, the most important integral length scale, which is the length scale in flow direction, could be determined in the experiments ($L_x = 0.065$ m). The two other length scales L_x and L_y were set to 0.02 m. In this way, a field $\mathcal{R}_x$ of correlated random numbers was obtained and the inflow condition was set to be

$$\mathbf{u}(t, -0.3, y, z) = \mathbf{u}_{\text{exp}}(-0.3, y, z) + \mathcal{R}_x(t, -0.3, y, z)\boldsymbol{\sigma}_{\text{exp}}(-0.3, y, z) \quad \text{in } (0, t_e) \times \Gamma_{\text{in}}.$$

Values at the inlet away from the measurement points were computed using bilinear interpolation. The second and third component of the inlet velocity were set to be zero.

Since measurement data for the flow field at the outflow boundary were not available, a standard outflow boundary condition, the do-nothing boundary condition,

$$(2\nu\mathbb{D}(\mathbf{u}) - p\mathbb{I})\,\mathbf{n}_{\partial\Omega} = \mathbf{0} \quad \text{in } (0, t_e) \times \Gamma_{\text{out}}$$

was used, where $\mathbf{n}_{\partial\Omega}$ denotes the unit normal vector and $\Gamma_{\text{out}} = \{0.5\} \times (-0.225, 0.225) \times (-0.18, 0)$. On all other boundaries, a free slip with penetration condition was applied in $(0, t_e)$

$$\mathbf{n}_{\partial\Omega} \cdot (2\nu\mathbb{D}(\mathbf{u}) - p\mathbb{I})\,\mathbf{n}_{\partial\Omega} = 0, \quad \boldsymbol{\tau}_{i,\partial\Omega} \cdot (2\nu\mathbb{D}(\mathbf{u}) - p\mathbb{I})\,\mathbf{n}_{\partial\Omega} = 0,\ i \in \{1, 2\}.$$

Here, $\{\boldsymbol{\tau}_{1,\partial\Omega}, \boldsymbol{\tau}_{2,\partial\Omega}\}$ is a system of orthonormal tangential vectors at the boundary. This choice of the boundary condition differs from the simulations without cylinder studied in Bordás et al. (2012, 2013a), where on the top boundary a symmetry condition was used. Clearly, for the turbulent vortex street, symmetry is not given.

The second equation of the population balance system models the droplet behavior

$$\partial_t f + \nabla_{\mathbf{x}} \cdot (f\,\mathbf{u}_{\text{drop}}) + \partial_d \left(\frac{a}{d} f\right) = C_+ + C_- \quad \text{in } (0, t_e) \times \Omega_{\text{DSD}} \times (d_{\min}, d_{\max}), \quad (2)$$

where f ($^{\text{no.}}/_{\text{m}^4}$) is the droplet size distribution, $d \in (d_{\min}, d_{\max})$ (m) is the internal coordinate (diameter of the droplets), $\mathbf{u}_{\text{drop}}$ ($^{\text{m}}/_{\text{s}}$) is the droplet velocity, $a = 5.0613 \cdot 10^{-12}$ $^{\text{m}^2}/_{\text{s}}$ the growth rate, C_+ the coalescence source, C_- the coalescence sink, and Ω_{DSD} the spatial domain in which the DSD was simulated.

For the well-posedness of (2), it is necessary to prescribe boundary conditions at the inlet. Since measurement data, which could be used for this purpose, were available only at the first measurement plane $x = 0$ m, the domain for simulating the DSD was chosen to be

$$\Omega_{\text{DSD}} = (0, 0.5) \times (-0.225, 0.225) \times (-0.18, 0)\ \text{m}^3.$$

At this plane, also data for the time-averaged air velocity $\mathbf{u}_{\text{air,exp}}(0,y,z)$ and the time-averaged droplet velocity $\mathbf{u}_{\text{drop,exp}}(0,y,z)$ were available. The experimental air velocity $\mathbf{u}_{\text{air,exp}}(0,y,z)$ was utilized for a comparison with the time-averaged air velocity that is obtained from the simulations, see Section 5. For defining $\mathbf{u}_{\text{drop}}$ in (2), both experimental data $\mathbf{u}_{\text{air,exp}}(0,y,z)$ and $\mathbf{u}_{\text{drop,exp}}(0,y,z)$ were extrapolated constantly into Ω_{DSD}, e.g., $\mathbf{u}_{\text{drop,exp}}(x,y,z) = \mathbf{u}_{\text{drop,exp}}(0,y,z)$ for all $(x,y,z) \in \Omega_{\text{DSD}}$. Then, the first component of the droplet velocity was defined by

$$(\mathbf{u}_{\text{drop}})_1(x,y,z) := \left(\mathbf{u}_{\text{drop,exp}} + \mathbf{u}_{\text{air,sim}} - \mathbf{u}_{\text{air,exp}}\right)_1(x,y,z).$$

The other two components of $\mathbf{u}_{\text{drop}}$ were set to be equal to the components coming from the numerical solution of (1). In this way, the simulated turbulent flow field determines the motion of the droplets.

The coalescence was modeled using the volume V of the droplets. Let f_V be the DSD and $C_{+,V}$, $C_{-,V}$ be source and sink, all with respect to the volume of the droplets. Then, the source term has the form proposed in Hulburt and Katz (1964)

$$C_{+,V} = \frac{1}{2}\int_0^V \kappa_{\text{col}}(V-V',V') f_V(V-V') f_V(V')\; dV'$$

and the sink term

$$\begin{aligned} C_{-,V} &= -\int_0^{V_{\max}} \kappa_{\text{col}}(V,V') f_V(V) f_V(V')\; dV' \\ &= -f_V(V)\int_0^{V_{\max}} \kappa_{\text{col}}(V,V') f_V(V')\; dV'. \end{aligned}$$

The choice of an appropriate collision kernel was discussed in detail in Bordás et al. (2013a). In particular, it was emphasized that in the wind tunnel experiments, unlike as, e.g., in clouds, a gravitational kernel can be neglected. Therefore, the combination of a standard Brownian motion kernel, which affects in particular small droplets, and a standard shear kernel, which has a strong influence on large droplets, was used

$$\begin{aligned} \kappa_{\text{col}}(V,V') &= C_{\text{brown}}\frac{2k_BT}{3\mu}\left(\sqrt[3]{V}+\sqrt[3]{V'}\right)\left(\frac{1}{\sqrt[3]{V}}+\frac{1}{\sqrt[3]{V'}}\right) \\ &\quad + C_{\text{shear}}\sqrt{2\nabla\mathbf{u}_{\text{drop}} : \nabla\mathbf{u}_{\text{drop}}}\left(\sqrt[3]{V}+\sqrt[3]{V'}\right)^3, \end{aligned} \tag{3}$$

where $k_B = 1.38\ 10^{-23}\ {}^{\text{J}}/_{\text{K}}$ is the Boltzmann constant and $\mu = 18.15\cdot 10^{-6}\ {}^{\text{kg}}/_{\text{ms}}$ is the dynamic viscosity. The model parameters C_{brown} and C_{shear} were unknown and they will be determined by calibrating experimental and numerical data.

Also equation (2) for the DSD has to be equipped with appropriate boundary and initial conditions. The choice of the boundary condition for the droplets at the inlet of Ω_{DSD} was based on experimental data. Measurements were performed at a grid of nodes at the first measurement plane $x = 0$ m. For a detailed description of the conversion of the experimental data to values for the DSD in these nodes, denoted by $f_{\text{in,exp}}(\mathbf{x},d)$, and the corresponding standard

deviation $\sigma_f(\mathbf{x}, d)$, it is referred to Bordás et al. (2012). The values in the nodes were interpolated to the whole measurement plane and the boundary condition was set to be

$$f(t, \mathbf{x}, d) = \begin{cases} f_{\text{in,exp}}(\mathbf{x}, d) + \text{rand}_{\text{normal}}(t, \mathbf{x})\sigma_f(\mathbf{x}, d), & \text{for } d \in [d_{\min}, d_{\max}], \\ 0, & \text{for } d \in [d_{\min,\text{art}}, d_{\min}), \end{cases} \tag{4}$$

with $\mathbf{x} = (0, y, z)$, $t \in [0, t_e]$, and $\text{rand}_{\text{normal}}$ denotes a normally distributed random variable. In (4), $d_{\min,\text{art}} = 0$ m is an artificial smallest diameter for the droplets that was introduced to define the necessary boundary condition with respect to the internal coordinate because of the positive growth rate, see Bordás et al. (2012) for a discussion of this topic. An initial distribution is not known from the experiments. Since the simulations were started with a fully developed flow field, the extrapolation of the experimental DSD from the first measurement plane to Ω_{DSD} was considered to be a reasonable approach for defining an initial condition. It should be noted already here that the time averaging of the data from the simulations started not at $t = 0$ s but after having allowed the system to develop for a while. Hence, the influence of the actual choice of the initial condition of the DSD on the time-averaged numerical results is expected to be negligible.

4 Numerical Methods

A number of numerical methods for solving the population balance system (1), (2) were explained in detail and studied comprehensively in Bordás et al. (2013a). Therefore, only a short presentation of the methods will be provided here and it is referred to Bordás et al. (2013a) for a detailed description.

All methods, which were studied in Bordás et al. (2013a), were also studied for the experiment considered in this paper, see Schmeyer (2013). For the sake of brevity, only the results for the best methods from Bordás et al. (2013a) will be presented here.

The general solution strategy for the population balance system was as follows. In each discrete time, first the Navier–Stokes equations (1) were solved and the flow field was computed. Then, the equation for the DSD (2) was solved, where the coalescence terms were always treated explicitly with respect to the DSD. With this approach, the problem in 4D became linear.

The turbulent flow field was simulated with a projection-based variational multiscale (VMS) method, which was introduced in John and Kaya (2005). More precisely, the version of the method which utilizes an adaptively chosen projection space presented in John and Kindl (2010) was applied. The Crank–Nicolson scheme was used as time stepping scheme and the inf-sup stable pair of finite element spaces Q_2/P_1^{disc} as spatial discretization.

For the discretization of the differential operator on the left-hand side of (2), three schemes were studied in Bordás et al. (2013a): a total variation diminishing essentially non-oscillatory (TVD-ENO) finite difference method from Shu and Osher (1988) and two linear flux-corrected transport methods with Crank–Nicolson time stepping (CN-FCT, CN-GFCT) proposed by Kuzmin (2009). The conclusion of Bordás et al. (2013a) was to recommend the TVD-ENO scheme, because it was the most efficient scheme and the finite element schemes were shown to introduce too much numerical diffusion if the convection field and the

grid are aligned. The strong alignment of the flow field and the grid was given in the channel flow studied in Bordás et al. (2013a). But this situation is not given for the turbulent vortex street studied here. Therefore, we think that it is of interest to present also results for the finite element schemes. Both considered schemes are of very similar accuracy, see John and Novo (2012). Thus, results will be presented only for the more efficient scheme, which is the group finite element version CN-GFCT.

A number of approaches were studied in Bordás et al. (2013a) for the evaluation of the integral terms on the right-hand side of the population balance equation (2). The recommendation of Bordás et al. (2013a) was a method proposed in Hackbusch (2006, 2007, 2009). This method requires the use of special grids with respect to the internal coordinate. They have to be piecewise equidistant with respect to the volume of the droplets. In these grids, the nodes did not coincide with the internal coordinates for which experimental data were available. Thus, an interpolation of the experimental data became necessary. In Bordás et al. (2013a), a linear interpolation and a log-normal interpolation were studied. It turned out that the experimental data could be reproduced better with the linear interpolation.

5 Results

5.1 Experiments

The velocity distribution of the air phase at the inlet plane ($x = 0$ m) was measured by means of Laser-Doppler Velocimetry (LDV). Measurements were carried out with a main flow velocity of $U = 2.32$ m/s, corresponding to a cylinder-based Reynolds number of $Re = UD/\nu = 3 \cdot 10^3$. During these measurements in the continuous phase, the nozzle was operating at the same pressure as in normal (spray) operation, but only with air and without water. Since the mass flow rate of air and water entering the nozzle are similar for normal operation conditions, only minor flow changes should be induced by this necessary operation.

In order to define the locations of the measurement points for the Laser-Doppler Velocimetry and the Phase-Doppler Anemometry (PDA) techniques, a measurement grid was generated with 874 (19 in z-direction $\times$ 46 in y-direction) measurement points, with 0.01 m distance in both directions between them. LDV and PDA measurements led to a high temporal resolution. Thus, the velocity components measured in the mean flow direction, Fig. 2, left, included the temporal fluctuations as well. In this way, the determination of the turbulence intensity was also possible, Fig. 2, right. The measured mean velocity of the air flow was $U = 2.45$ m/s. Based on U and on the hydraulic diameter of the wind tunnel ($D_H = 0.5454$ m), the Reynolds number of the flow is $8 \cdot 10^4$. The measured fluctuation of the air flow velocity in main flow direction was in the average $u' = 0.33$ m/s. This leads to a mean turbulence intensity of 15%. The energy cascade of a turbulent flow can be estimated by post-processing the measurement results. The resulting Kolmogorov length scale is $2 \cdot 10^{-4}$ m, as shown in Bordás et al. (2013b).

The properties of the disperse phase (water spray) were then measured separately in the three vertical planes at $x = 0$ m, $x = 0.2$ m, and $x = 0.4$ m, using

the same measurement grid as previously. Velocities measured by PDA are based on the same principles as LDV. However, using PDA, the simultaneous measurement of the diameter and the velocity values was possible. Calculating the droplet Stokes number St from the droplet properties, the Kolmogorov length scale and the RMS velocity fluctuations, the most frequent value of $St = 2 \cdot 10^{-3}$ in a range of $St = 10^{-3} \ldots 10^{2}$ was found.

At the outlet boundary ($x = 0.4$ m), experimental data were needed as well for comparison purposes. Therefore, a corresponding postprocessing of the PDA measurements was necessary to obtain values for the number density or droplet concentration. These calculations were performed in the same manner as described, e.g., in Bordás et al. (2012), resulting in the droplet concentration as a function of the droplet diameter, together with the corresponding standard deviation.

5.2 Numerical Simulations and Comparison with the Experimental Data

All simulations were performed in the time interval $[0, 1]$ s. In $[0, 0.5]$ s, the system was allowed to develop and time-averaging of data was performed in $[0.5, 1]$ s. In particular, all droplets injected at $t = 0$ s had already left the domain before the start of the time-averaging.

The grid for Ω_{NSE} is presented in Fig. 3. On this grid, there were 973 728 degrees of freedom for the velocity and 156 032 degrees of freedom for the pressure. The grid is refined in the domain around and behind the cylinder since most of the turbulence can be expected in these regions. The grid for Ω_{DSD} was just the right part of the grid for Ω_{NSE}, starting at $x = 0$ m. All measurement points were nodes of the grid. For the internal coordinate, an appropriate grid for the method for evaluating the coalescence integrals was chosen which had 94 nodes. Altogether, there were 4 086 650 degrees of freedom for the TVD-ENO and CN-GFCT discretizations of the DSD equation. The length of the time step was always set to be $\Delta t = 10^{-3}$ s.

The simulations were performed with the research code MooNMD John and Matthies (2004).

First, the flow field will be considered. Behind the cylinder, a turbulent Kármán vortex street is developing, see Fig. 4. As already mentioned above, experimental data for the time-averaged velocity component in flow direction were available at the plane $x = 0$ m, see Fig. 2. In Fig. 5, the time-averaged velocity that was obtained in the simulations at $x = 0$ m is shown. One can observe a very good agreement. The values are in the same range and the slight asymmetry observed experimentally is well reproduced. Thus, one can conclude that the choice of the inlet condition as described in Section 3 was appropriate and also that the simulation of the turbulent flow field with the VMS method was accurate, at least with respect to the time-averaged velocity.

Concerning the DSD, the first goal was the determination of suitable parameters C_{brown} and C_{shear} in the collision kernel (3). Because of the turbulent nature of the flow, the time-averaged experimental data were different in different measurement points. Therefore, a spatial averaging was applied. The same strategy was used in the numerical simulations.

The calibration of the model parameters was performed by trial and error using the method TVD-ENO. It turned out that a good fit between experimen-

tal and numerical results was obtained for $C_{\text{brown}} = 10^5$ and $C_{\text{shear}} = 30$, see Fig. 6. Comparing these parameters with the parameters found for the channel flow in Bordás et al. (2012), one can observe some differences. For the channel flow, $C_{\text{shear}} = 0.1$ was found to be appropriate, but it was also noted that this parameter has only little influence. We checked that with $C_{\text{shear}} = 30$ one obtains for the channel flow almost the same results as for $C_{\text{shear}} = 0.1$. Thus, C_{shear} can be calibrated in the same way for both situations. The other parameter was $C_{\text{brown}} = 1.5 \cdot 10^6$ for the channel flow. Thus there is a difference of one order of magnitude. There is most probably some uncertainty in the experimental data which might contribute to having obtained different parameters. Difficulties with the measurement of small droplets, with diameter less than 15 μm, and the development of an appropriate collision kernel have been reported also recently in Siewert et al. (2013). However, the modeling question of an appropriate collision kernel is outside the scope of this paper.

Results obtained with the two numerical methods for discretizing the left-hand side of the DSD equation (2) are presented in Fig. 7. One can observe that the curve obtained with CN-GFCT is somewhat below the curve computed with TVD-ENO. This result is similar to the observation for the turbulent channel flow from Bordás et al. (2013a). Thus, even if the vortex street is not that closely aligned to the grid as the channel flow, CN-GFCT behaves similarly for both situations. This method seems still to introduce too much numerical diffusion, a feature which was identified in Bordás et al. (2013a) for the case that grid and convection are aligned.

The simulations were performed on a compute server HP BL680c G7 2xXeon, Ten-Core 2400MHz. For one time step, solving the Navier–Stokes equations took around 125 seconds, computing the coalescence integrals nearly 30 seconds, applying TVD-ENO around 5 seconds, and CN-GFCT about 45 seconds.

Finally, the impact of different turbulent flows on the same DSD is studied in a model situation. To this end, the turbulent channel flow considered in Bordás et al. (2012, 2013a) and the turbulent vortex street presented in this paper were used. Concerning the DSD, three isolated diameters were chosen, $d_{\text{small}} = 9 \times 10^{-6} m$, $d_{\text{middle}} = 19 \times 10^{-6} m$, and $d_{\text{large}} = 39 \times 10^{-6} m$. At the inlet, the value of the DSD was set to be 10^3 ($^{\text{no.}}/_{\text{m}^4}$) for these diameters in all nodes. All other inlet values of f were set to be zero. The simulations were performed with TVD-ENO, $C_{\text{brown}} = 10^5$, and $C_{\text{shear}} = 30$. The resulting DSD at the outlet is presented in Fig. 8. One can observe that the number of droplets for the considered diameters is smaller for the turbulent vortex street. On the other hand, one can see clearly that for d_{middle} and d_{large} more droplets with larger diameters are created, due to coalescence, for the turbulent vortex street. This observation corresponds to the expectation that in the turbulent vortex street there are more collisions of droplets and therefore eventually more successful coalescence processes occur.

6 Summary and Outlook

This paper studied the behavior of a disperse droplet population in a turbulent air flow. Inserting a cylinder into a wind tunnel, a turbulent vortex street was generated. Data of the velocities of air and droplets were obtained by non-intrusive measurement techniques. The process was modeled with a population

balance system. Simulations of this model were performed by using modern numerical methods. Two unknown model parameters had to be calibrated. Very good agreements between experimental and numerical data could be observed for the mean velocity in a cut plane and for the space-time averaged droplet size distribution at the outlet.

A possible improvement of the collision kernel for the coalescence integrals should be considered in future. The calibration of one of the parameters resulted in a different order of magnitude for the considered vortex street and a channel flow in previous simulations. Concerning the numerical methods, a better understanding and improvement of CN-GFCT would be desirable. This method can be applied, in contrast to TVD-ENO, not only on tensor-product meshes. From this point of view, CN-GFCT would be a potential method to be used if general spatial domains are considered.

Acknowledgments

The funding of this project in the framework of the priority program SPP 1276 MetStröm: Multiple Scales in Fluid Mechanics and Meteorology, by the German Research Foundation (DFG) is gratefully acknowledged. E. Schmeyer was founded under grant number Jo329/8-3 and R. Bordás under grant number Th881/13-3.

References

Bordás, R., T. Hagemeier, B. Wunderlich, and D. Thévenin, 2011: Droplet collisions and interaction with the turbulent flow within a two-phase wind tunnel. *Physics of Fluids*, **23 (085105)**, 1–11.

Bordás, R., V. John, E. Schmeyer, and D. Thévenin, 2012: Measurement and simulation of a droplet population in a turbulent flow field. *Computers & Fluids*, **66 (0)**, 52 – 62.

Bordás, R., V. John, E. Schmeyer, and D. Thévenin, 2013a: Numerical methods for the simulation of a coalescence-driven droplet size distribution. *Theoretical and Computational Fluid Dynamics*, **27 (3-4)**, 253–271.

Bordás, R., C. Roloff, D. Thévenin, and R. A. Shaw, 2013b: Experimental determination of droplet collision rates in turbulence. *New Journal of Physics*, **15 (4)**, 045 010.

Ganesan, S. and L. Tobiska, 2012: An operator-splitting finite element method for the efficient parallel solution of multidimensional population balance systems. *Chem. Eng. Sci.*, **69 (1)**, 59 – 68.

Hackbusch, W., 2006: On the efficient evaluation of coalescence integrals in population balance models. *Computing*, **78 (2)**, 145–159.

Hackbusch, W., 2007: Approximation of coalescence integrals in population balance models with local mass conservation. *Numer. Math.*, **106 (4)**, 627–657.

Hackbusch, W., 2009: Convolution of *hp*-functions on locally refined grids. *IMA J. Numer. Anal.*, **29 (4)**, 960–985.

Hackbusch, W., V. John, A. Khachatryan, and C. Suciu, 2012: A numerical method for the simulation of an aggregation-driven population balance system. *Internat. J. Numer. Methods Fluids*, **69 (10)**, 1646–1660.

Hulburt, H. and S. Katz, 1964: Some problems in particle technology – a statistical mechanical formulation. *Chem. Engrg. Sci.*, **19**, 555 – 574.

John, V. and S. Kaya, 2005: A finite element variational multiscale method for the Navier-Stokes equations. *SIAM J. Sci. Comput.*, **26 (5)**, 1485–1503.

John, V. and A. Kindl, 2010: A variational multiscale method for turbulent flow simulation with adaptive large scale space. *J. Comput. Phys.*, **229 (2)**, 301–312.

John, V. and G. Matthies, 2004: MooNMD—a program package based on mapped finite element methods. *Comput. Vis. Sci.*, **6 (2-3)**, 163–169.

John, V. and J. Novo, 2012: On (essentially) non-oscillatory discretizations of evolutionary convection-diffusion equations. *J. Comput. Phys.*, **231 (4)**, 1570–1586.

Klein, M., A. Sadiki, and J. Janicka, 2003: A digital filter based generation of inflow data for spatially developing direct numerical or large eddy simulations. *Journal of Computational Physics*, **186 (2)**, 652 – 665.

Kuzmin, D., 2009: Explicit and implicit FEM-FCT algorithms with flux linearization. *J. Comput. Phys.*, **228 (7)**, 2517–2534.

Marchisio, D. L. and R. O. Fox, 2005: Solution of population balance equations using the direct quadrature method of moments. *Journal of Aerosol Science*, **36 (1)**, 43 – 73.

Schmeyer, E., 2013: Numerische verfahren zur simulation von mehrphasenströmungen mittels populationsbilanzen. Ph.D. thesis, Freie Universität Berlin.

Shu, C.-W. and S. Osher, 1988: Efficient implementation of essentially nonoscillatory shock-capturing schemes. *J. Comput. Phys.*, **77 (2)**, 439–471.

Siewert, C., R. Bordás, U. Wacker, K. Beheng, R. P. Kunnen, S. Wolfgang, and D. Thévenin, 2013: Influence of turbulence on the drop growth in warm clouds, part I: Comparison of numerically and experimentally determined collision kernels. Tech. rep. Submitted to Meteorologische Zeitschrift.

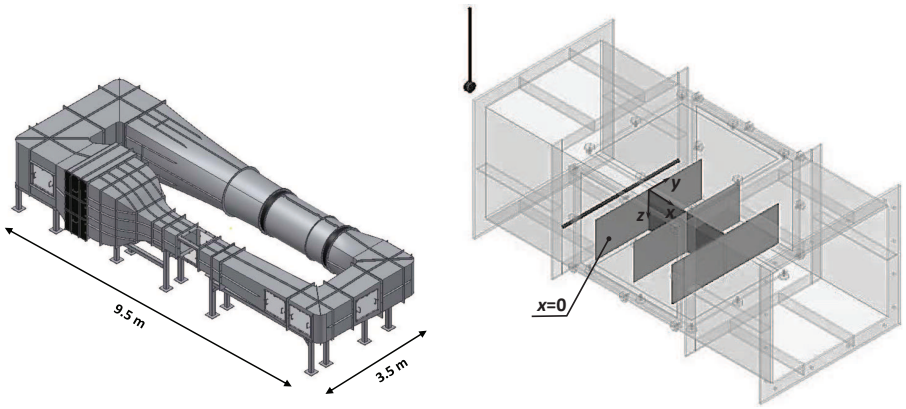

Figure 1: Two-phase Prandtl wind tunnel with closed test section (left), measurement section with counter-flow droplet injection and a cylindrical bluff body right before the test section (right).

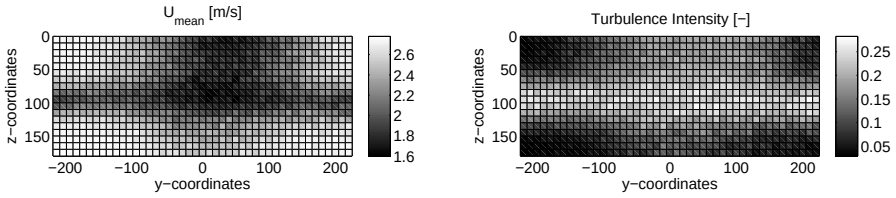

Figure 2: Mean longitudinal velocity distribution in the plane of $x = 0$ m (left), turbulence intensity distribution in the plane of $x = 0$ m (right).

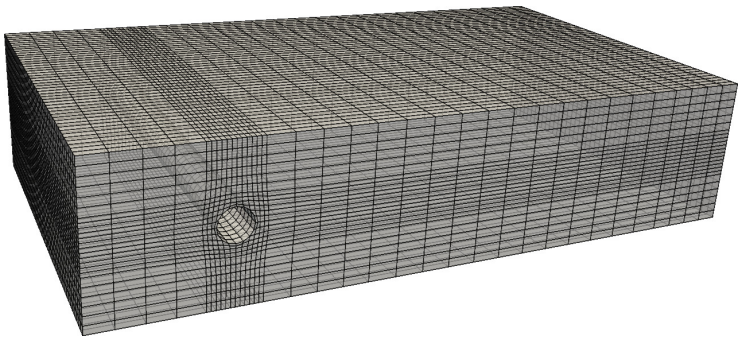

Figure 3: Grid for the simulations.

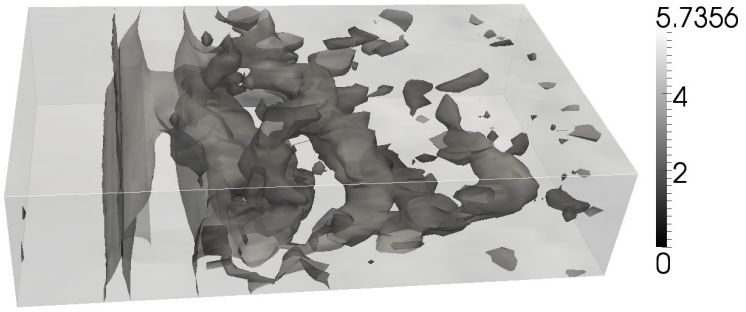

Figure 4: Snapshot of the simulated flow field, iso-surfaces of the pressure for two values.

Figure 5: Time-averaged first component of the velocity from the simulations.

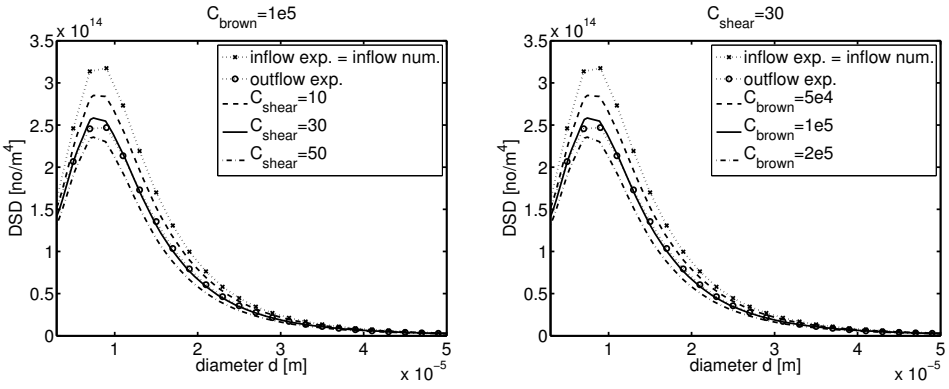

Figure 6: Calibration of the model parameters C_{brown} and C_{shear}, simulations with TVD-ENO.

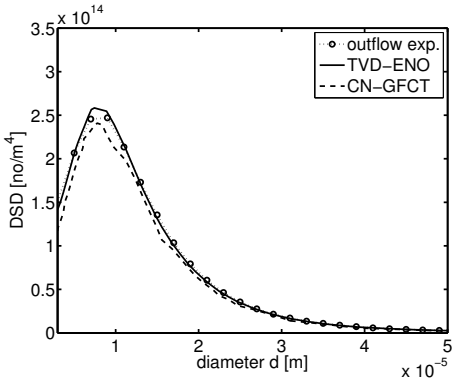

Figure 7: Comparison of results with different discretizations of the DSD equation (2), $C_{\text{brown}} = 10^5$, $C_{\text{shear}} = 30$.

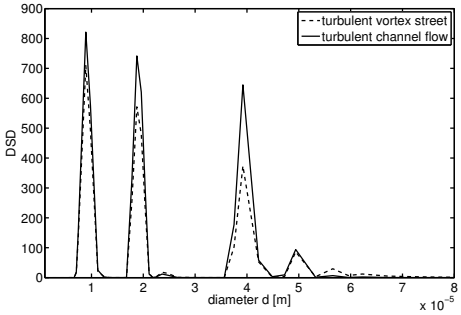

Figure 8: Effect of different turbulent flows on certain droplets with different diameters, TVD-ENO, $C_{\text{brown}} = 10^5$, $C_{\text{shear}} = 30$.